Original Article

Institution of MECHANICAL ENGINEERS
Journal of ENGINEERING TRIBOLOGY

Proc IMechE Part J:
J Engineering Tribology
2015, Vol. 229(10) 1239–1246

DOI: 10.1177/1350650115576783
pij.sagepub.com
SAGE

Effects of frictional material properties on thermoelastic instability deformation modes

Jiaxin Zhao[1], Yun-Bo Yi[1] and Heyan Li[2]

Abstract

This paper deals with the effects of friction material properties on thermoelastic instability (TEI) and the associated dominant deformation mode. Both analytical and finite element models are constructed for determining the variation of the critical speed and the dominant TEI mode. Some important factors, e.g. the nonconductive friction material as well as the symmetric and anti-symmetric TEI deformation modes, are investigated. It has been found that the dominant TEI deformation mode is strongly dependent on the properties of frictional material. The results show that the symmetric mode can be dominant in the condition when the friction material has either a sufficiently large elastic modulus or a sufficiently small thermal conductivity. These research findings are useful for vehicle clutch and brake designs.

Keywords

Thermoelastic instability, deformation modes, critical speed, material properties, finite element method

Date received: 18 September 2014; accepted: 12 February 2015

Introduction

In vehicle frictional components, e.g. brakes and clutches, hot spots are believed to be a main cause of surface failures. In view of the thermoelastic instability (TEI) theory, hot spots are induced by the unstable behavior of a frictional system. To explain it further, during the engagement of friction components, various physical fields, e.g. the frictional heat, the thermal deformation, the thermal stress, the contact pressure, and the temperature field experience intense interactions. In some extreme cases, when the sliding speed of the friction pair exceeds a critical value, the physical fields become unstable and the initial variations can grow exponentially with time, which leads to local areas with high temperature and strong contact pressure. The TEI theory has been widely accepted and been demonstrated by different methods, i.e. the analytical studies,[1–5] the experimental researches,[6,7] and the finite element (FE) investigations.[8–12]

During the frictional process, two representative TEI deformation modes of the metal material can occur, i.e. the symmetric mode and the anti-symmetric mode that are shown in Figure 1. As the unstable behaviors under different modes are dissimilar, the investigation on the deformation mode is a fundamental and key issue in the TEI research. In general, we define the dominant mode as the TEI deformation mode with the lowest critical speed. Lee[13] provided an analytical method to study the TEI deformation modes and predicted that the anti-symmetric mode was the dominant mode for two materials, i.e. the asbestos-based material and the semi-metallic material. On the basis of this conclusion, most of the previous TEI researches[14–16] focused on the unstable behavior under the anti-symmetric mode. Whereas the study of the symmetric modes has been lacking in the literature.

In the present paper, we will develop a FE method to overcome the difficulties in the analytical approach involving numerical iterations. The intent of this work is to investigate the unstable behavior under the symmetric TEI deformation mode and to demonstrate the possibility that the symmetric mode can be dominant in some situations.

[1]Department of Mechanical and Materials Engineering, University of Denver, Denver, USA
[2]School of Mechanical Engineering, Beijing Institute of Technology, Beijing, China

Corresponding author:
Jiaxin Zhao, Department of Mechanical and Materials Engineering, University of Denver, 2199 S University Blvd, Denver, CO 80208, Denver, USA.
Email: jiaxin1773@gmail.com

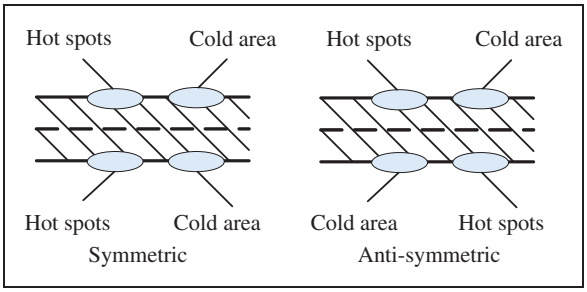

Figure 1. TEI deformation modes.

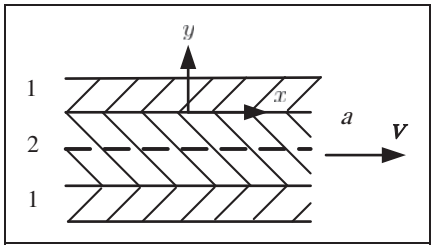

Figure 2. Schematic diagram of the two-dimensional FE model.

Finite element approaches

2D finite element model

We consider two half planes that are composed of a friction material in body 1, sliding on a metal plane of body 2 with a finite thickness $2a$, as shown in Figure 2.

In the schematic, the finite thickness plane moves at a velocity V to the right side while two half planes are stationary. Different bodies are pressed together by external pressure. In the same diagram, a coordinate system (x,y) moving with the pressure perturbation field is also introduced. To present a temperature perturbation, we assume a spatially cosine function that grows exponentially with time, which can be written as

$$\begin{aligned} T &= U_j(y)\cos(\lambda x)\exp(bt) \\ &= \Re\{U_j(y)\exp(bt + i\lambda x)\} \end{aligned} \tag{1}$$

where T, U, b, λ are, respectively, the temperature perturbation, the temperature function, the growth rate, and the spatial frequency of the temperature perturbation, $j = 1,2$.

To find the corresponding growth rates for different sliding speeds, a commonly used FE method, i.e. the Galerkin method, is applied. The details of the FE formulation can be found in Yi's paper,[10] which gives a matrix equation as

$$(\boldsymbol{K} + \boldsymbol{C} + fV\boldsymbol{GB} + b\boldsymbol{H})\boldsymbol{U} = 0 \tag{2}$$

Where

$$\boldsymbol{K} = \int_\Omega K_j\left(\frac{\mathrm{d}\boldsymbol{W}}{\mathrm{d}y}\frac{\mathrm{d}\boldsymbol{W}^{\mathrm{T}}}{\mathrm{d}y}\right)\mathrm{d}\Omega$$

$$\boldsymbol{C} = \int_\Omega (K_j\lambda^2 + \mathrm{i}\lambda V_j\rho_j c_{pj})\boldsymbol{W}\boldsymbol{W}^{\mathrm{T}}\mathrm{d}\Omega$$

$$\boldsymbol{H} = \int_\Omega \rho_j c_{pj}\boldsymbol{W}\boldsymbol{W}^{\mathrm{T}}\mathrm{d}\Omega$$

$$\boldsymbol{G} = \begin{bmatrix} \boldsymbol{I} \\ 0 \end{bmatrix}$$

where f, K_j, ρ_j, c_{pj}, Ω are, respectively, the friction coefficient, the thermal conductivity, the density, the specific heat, and the combined line of two bodies. $\boldsymbol{B}$, $\boldsymbol{U}$, $\boldsymbol{I}$ represent, respectively, the transition matrix, the temperature matrix, and the identity matrix.

Equation (2) is equivalent to

$$\boldsymbol{SU} = b\boldsymbol{U} \tag{3}$$

where

$$\boldsymbol{S} = -\boldsymbol{H}^{-1}(\boldsymbol{K} + \boldsymbol{C} + fV\boldsymbol{GB})$$

If the sliding speed V is given and the transition matrix $\boldsymbol{B}$ is known, the growth rate b can be found from the eigenvalues of the $N \times N$ matrix $\boldsymbol{S}$. The most efficient approach to determine the transition matrix $\boldsymbol{B}$ is to write a custom-made FE code of the thermoelastic problem in which the Fourier term can be deleted before discretization.[10] With the FE program, the growth rates at different sliding speeds can be deduced. When the growth rate $b = 0$, the corresponding sliding speed is the critical speed.

Boundary conditions

To solve the eigenvalue problem, a set of boundary conditions, e.g. the heat flux and the thermal stresses must be imposed on the interface. The frictional heat at the interface of the two bodies can be written as

$$q = fV_p \tag{4}$$

where q, p represent, respectively, the heat flux and the contact pressure. The heat flux of body j has a relationship with the temperature field, as

$$q_j = -K_j\frac{\partial T_j}{\partial y} \tag{5}$$

Consequently, the energy balance at the interface is

$$K_2\frac{\partial T_2}{\partial y} - K_1\frac{\partial T_1}{\partial y} = fV_p \tag{6}$$

Two representative thermoelastic deformation modes of body 2 can occur when the system is

under unstable condition. Hot spots appear on the same position of both sides under the symmetric mode, shown in Figure 1. Hence, the boundary conditions for the symmetric mode can be expressed as

$$\begin{aligned} &y = -a; \quad q_2 = 0; \\ &u_{y2} = 0; \quad \tau_{xy2} = 0 \end{aligned} \tag{7}$$

where u_y, τ_{xy} are, respectively, the thermoelastic displacement in the y-direction and the shear stress. Furthermore, hot spots are spaced alternatively on two sides under the anti-symmetric mode. Consequently, the boundary conditions for the anti-symmetric mode can be written as

$$\begin{aligned} &y = -a; \quad T_2 = 0; \\ &u_{x2} = 0; \quad \sigma_{y2} = 0 \end{aligned} \tag{8}$$

where u_x, σ_y are, respectively, the thermoelastic displacement in the x-direction and the normal stress in the y-direction.

Special cases

Nonconductive friction material

The analytical model used in this section is based on Lee's paper[13] with some modifications. Those equations originally developed by Lee are not repeated here to avoid redundancy. Here, we define $A = \lambda a$ as the dimensionless wave number. When the friction material is a nonconductor, i.e. $K_1 = 0$, the perturbation becomes stationary in the metal material and therefore the solution can be simplified. After some mathematical simplification on Lee's model, we obtain the following symmetric solution

$$\begin{aligned} \frac{\sinh(2A)}{\cosh(2A)+1} &= \frac{fH_1V^*}{2}\left[\frac{\alpha^*}{\xi_1^*}(A\operatorname{sech}^2 A + \tanh A)\right] \\ &\quad + \frac{\tanh A(\sinh(2A)+2A)}{\cosh(2A)+1} \end{aligned} \tag{9}$$

where

$$\begin{aligned} H_1 &= \frac{2\mu_1\mu_2k_2\alpha_2(1+\nu_2)}{M} \\ M &= [\mu_2(1-\nu_1)(A\operatorname{sech}^2 A \\ &\quad + \tanh A) + \mu_1(1-\nu_2)\tanh^2 A]K_2 \end{aligned} \tag{10}$$

where μ, k, α, ν are, respectively, the shear modulus, the thermal diffusivity, the thermal expansion coefficient, Poisson's ratio of the materials.

This is a degenerate nonlinear equation in the sense that the solution V^* is determined by a single variable equation instead of two equations in the original Lee's model.

Similarly the degenerate anti-symmetric solution for $K_1 = 0$ is determined from

$$\begin{aligned} \frac{\sinh(2A)}{\cosh(2A)-1} &= \frac{fH_1'V^*}{2}\left[\frac{\alpha^*}{\xi_1^*}(-A\operatorname{csch}^2 A + \coth A)\right] \\ &\quad + \frac{\cosh A(\sinh(2A)-2A)}{\cosh(2A)-1} \end{aligned} \tag{11}$$

where

$$\begin{aligned} H_1' &= \frac{2\mu_1\mu_2k_2\alpha_2(1+\nu_2)}{M'} \\ M' &= [\mu_2(1-\nu_1)(-A\operatorname{csch}^2 A \\ &\quad + \coth A) + \mu_1(1-\nu_2)\coth^2 A]K_2 \end{aligned} \tag{12}$$

In both cases

$$\alpha^* = \frac{\alpha_1(1+\nu_1)}{\alpha_2(1+\nu_2)} \tag{13}$$

$$\xi_1^* = \frac{1}{2}\left[1 + \sqrt{1 + \left(\frac{V^*}{k^*}\right)^2}\right]^{\frac{1}{2}} \tag{14}$$

$$\frac{V_a}{k_2} = V^*A \tag{16}$$

$$k^* = \frac{k_1}{k_2} \tag{17}$$

Asymptotic solution for large A

When A is sufficiently large, in a general situation for $K_1 > 0$, equation (68) in Lee's paper can be reduced to

$$\begin{aligned} &K^*\xi_1^* + \xi_2^* + f\frac{H_1}{H_2}(K^*\eta_1^* + \eta_2^*) = \\ &\frac{fH_1V^*}{2}\left(\frac{\alpha^*}{\xi_1^*} + \frac{1}{\xi_2^*}\right) \end{aligned} \tag{18}$$

and equation (69) in Lee's paper becomes

$$\begin{aligned} &K^*\eta_1^* + \eta_2^* - f\frac{H_1}{H_2}(K^*\xi_1^* + \xi_2^*) = \\ &-\frac{fH_1V^*}{2}\left(\frac{\alpha^*\eta_1^*}{\xi_1^*(\xi_1^*+1)} + \frac{\xi_2^*-1}{\xi_2^*\eta_2^*}\right) \end{aligned} \tag{19}$$

where

$$\xi_1^* = \sqrt{1+\eta_1^{*2}}$$

$$\xi_2^* = \sqrt{1+\eta_2^{*2}}$$

The solution for V^* can therefore be obtained by solving equations (18) and (19) simultaneously, using the following relationship

$$V^* = k^* \sqrt{\left(2\eta_1^{*2} + 1\right)^2 - 1} + \sqrt{\left(2\eta_2^{*2} + 1\right)^2 - 1} \tag{20}$$

Results

Convergence

To validate the convergence of the FE analysis, we first apply the same materials as those in Lee's research.[13] All material properties are specified in Table 1.

In the FE progress, we define the friction coefficient $f = 0.4$, the half thickness $a = 10$ mm, and the thickness of body 1 as 200 mm to represent the semi-infinite thickness. A comparison between the analytical solution and the FE solution (anti-symmetric mode) is illustrated in Figure 3. The figure shows an excellent agreement between the two solutions.

We also investigated the symmetric solutions, using both the original Lee's solutions and the FE solutions. The symmetric solutions at lower values of K_1 were successfully obtained and presented in Figure 4. However, we encountered some numerical convergence problems in search of Lee's solution at higher K_1 values (>0.3 W/m °C). In Figure 4, the analytical solution is validated by the FE solution using several different values of the frication material thickness. It can be seen that the analytical and FE solutions consistently agree well for larger wave numbers. At lower wave numbers, however, the FE solution has an initial uphill region due to the geometric effect of the finite friction material thickness. As the friction material thickness increases, the FE solution gradually approaches Lee's solution with a good convergence. Consequently, we can conclude that the original Lee's analytical symmetric solutions are inaccurate at lower wave numbers. Therefore an improved method, i.e. the FE method, is entailed to study the unstable behavior under the symmetric mode along with the dominant deformed shape.

Table 1. Material properties.

Material	Cast iron	Material A	Material B
E (GPa)	125	0.53	1
ν	0.25	0.25	0.25
α (°C^{-1})	1.2×10^{-5}	3×10^{-5}	1×10^{-5}
K (W/m°C)	54	0.5	5
k (m^2/s)	12.98×10^{-6}	2.69×10^{-5}	3.57×10^{-6}

Nonconductive friction material

To begin with the discussion, we first investigate the dominant deformation mode for nonconductive friction materials. When the friction material is a thermal insulator, the analytical solutions and the FE solutions under the anti-symmetric mode show an excellent agreement in Figure 5. The result exhibits some similar trends in comparison with the case of conductive friction material, e.g. the dimensionless critical speed decreases at the beginning, reaches a minimum value, and then increases with the wave number.

The symmetric solutions are shown Figure 6. Again, the analytical and FE solutions agree with each other very well. It can be seen that the dimensionless critical speed for $K_1 = 0$ increases almost linearly with the dimensionless wave number A, showing a behavior entirely different from those involving

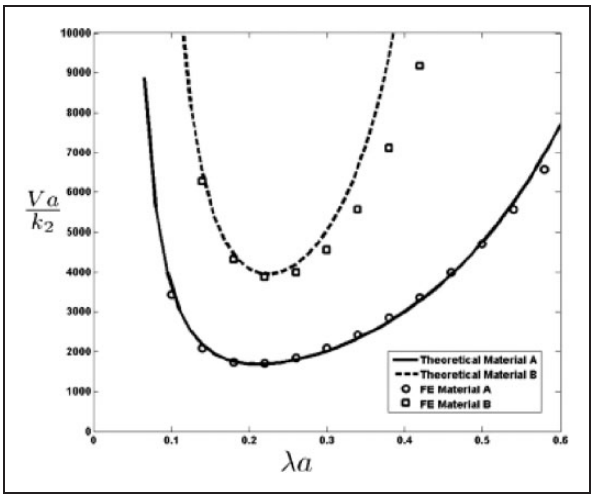

Figure 3. Dimensionless critical speed under the anti-symmetric mode.
FE: finite element.

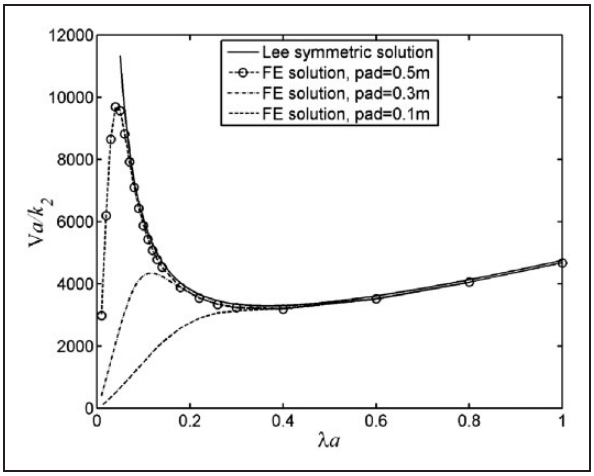

Figure 4. Dimensionless critical speed under the symmetric mode.
FE: finite element.

conductive friction material. In comparison with Figure 5, the critical speed in Figure 6 is consistently lower, implying that the symmetric modes become dominant when the conductivity of the friction material approaches zero.

Thermal conductivity

The frictional material design is used for improving the performance of the frictional system. Meanwhile, the material optimization can also contribute to the mitigation of TEI-induced hot spots. We keep other parameters unchanged (Material A), except for the thermal conductivity as $K_1 = 0.5,\ 0.6,\ 0.7\,\mathrm{W/m^{\circ}C}$. The critical speeds under the two deformation modes are presented in Figure 7. When the thermal conductivity of the friction material increases, the critical speeds under both modes decrease accordingly. An explanation is that the heat distribution is more uniform when the friction material has a higher thermal conductivity.

Meanwhile, the growth rates of critical speeds under the two modes are significantly different, e.g. when thermal conductivity increases from $0.5\,\mathrm{W/m^{\circ}C}$ to $0.6\,\mathrm{W/m^{\circ}C}$, the growth rates of the anti-symmetric mode and the symmetric mode are, respectively, 20.6% and 30.3% ($\lambda a = 0.6$). In addition, as mentioned before, the symmetric mode is dominant when the friction material is a thermal insulator. Therefore a different behavior of friction material with a low thermal conductivity can be expected.

We select small values of thermal conductivity as $K_1 = 1 \times 10^{-4},\ 1 \times 10^{-3}\,\mathrm{W/m^{\circ}C}$, and the relevant critical speeds are shown in Figure 8. Apparently, the symmetric TEI mode can be predominant when the friction material has a sufficiently small

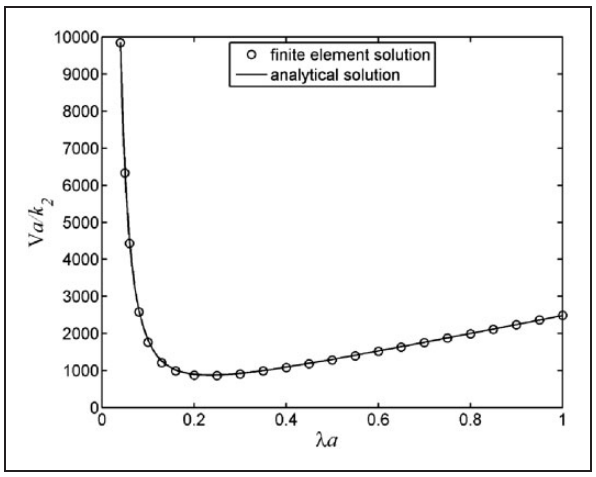

Figure 5. Anti-symmetric solution for nonconductive friction material.

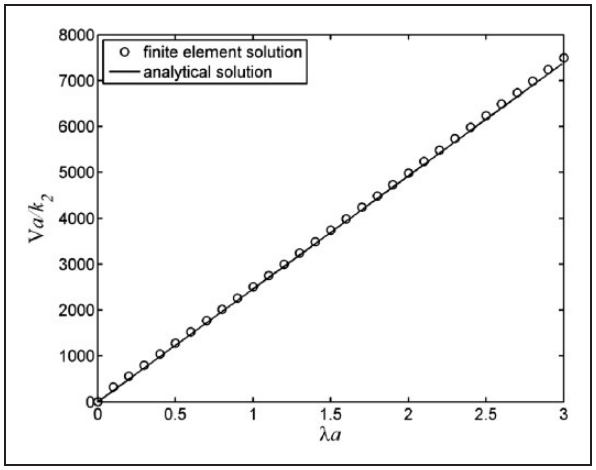

Figure 6. Symmetric solution for nonconductive friction material.

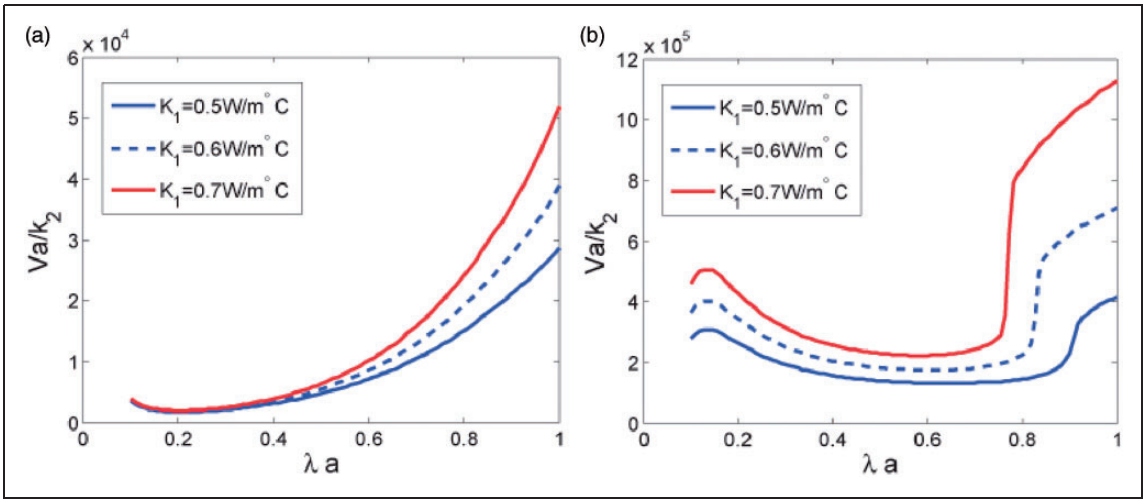

Figure 7. Effect of thermal conductivity of the friction material on the critical speed: (a) anti-symmetric; (b) symmetric.

thermal conductivity. In Figure 8, the transient point of the two deformation modes is $\lambda a = 0.25$ when $K_1 = 1 \times 10^{-3}$ W/m°C and $\lambda a = 0.52$ when $K_1 = 1 \times 10^{-4}$ W/m°C. Additionally, the dominant region of the symmetric mode is larger with the smaller thermal conductivity, e.g. when $K_1 = 1 \times 10^{-3}$ W/m°C, the dominant region is $\lambda a = 0$–0.25, when $K_1 = 1 \times 10^{-4}$ W/m°C, the dominant region is $\lambda a = 0$–0.52.

Elastic modulus

Another important factor related to the system instability is the elastic modulus. According to the analytical work[13] and the experimental data,[6] under the anti-symmetric mode, hot spots are discouraged when the friction material has a low elastic modulus. Similarly, we maintain the friction material parameters constant except the elastic modulus ($E_1 = 0.53$, 0.58, 0.63 GP). The corresponding critical speeds calculated by the FE analysis are illustrated in Figure 9.

Apparently, the elastic modulus has a similar effect on the critical speed under the two deformation modes. When the elastic modulus increases, the critical speed decreases as a result of the uniformity of the contact pressure at the interface.

It is also noteworthy that the elastic modulus of friction material A shown in Table 1 is only 0.53 GPa. However, the elastic modulus of typical frictional materials can be up to 10 GPa.[17] To investigate the unstable behavior of friction materials with large elastic modulus, we apply elastic modulus as $E_1 = 4$, 6 GPa and then exhibit the corresponding critical speeds in Figure 10.

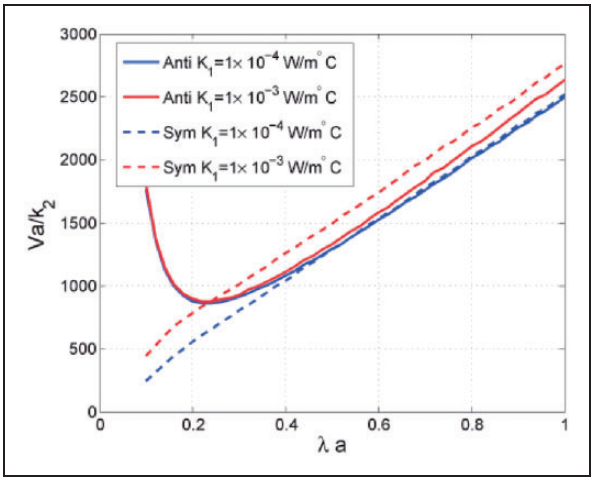

Figure 8. Critical speeds under two deformation modes with small friction material thermal conductivity.

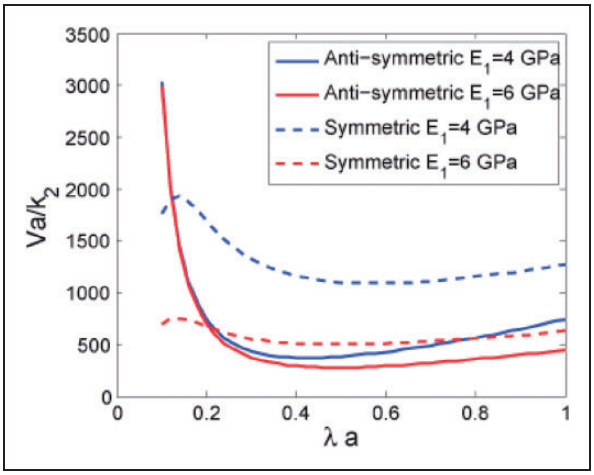

Figure 10. Critical speeds under two deformation modes with large friction material elastic modulus.

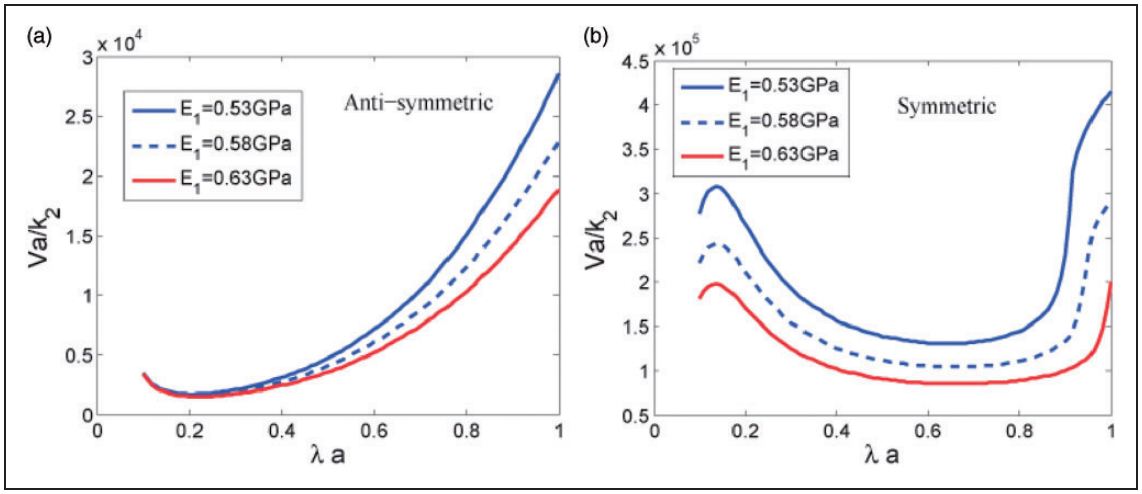

Figure 9. Effect of elastic modulus of the friction material on the critical speed: (a) anti-symmetric; (b) symmetric.

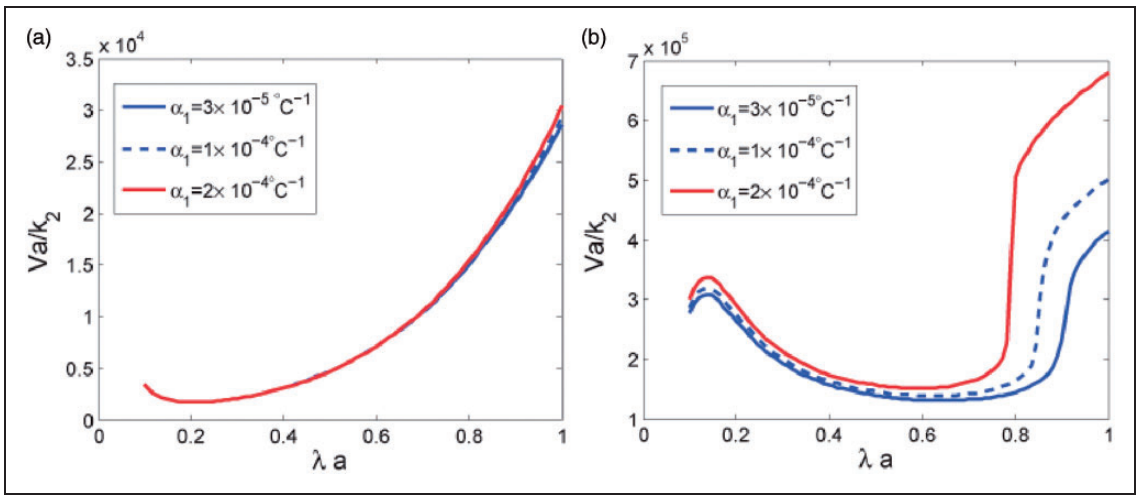

Figure 11. Effect of thermal expansion coefficient of the friction material on the critical speed: (a) anti-symmetric; (b) symmetric.

Two important conclusions can be obtained from Figure 10. Primarily, the symmetric deformation mode becomes dominant when the elastic modulus of the friction material is sufficiently large, e.g. $E_1 = 4$ GPa, the symmetric solution is lower in the range $\lambda a = 0$–0.12.

Secondly, a transient mode from the symmetric mode to the anti-symmetric mode may appear during the frictional process. In Figure 10, the transient moments are $\lambda a = 0.12$ for 4 GPa and $\lambda a = 0.22$ for 6 GPa. Consequently, the unstable behavior of frictional materials with large elastic modulus is disparate and the symmetric deformation mode can be the dominant one.

Thermal expansion coefficient

Thermal expansion is the trend to change volume in response to the variation of the temperature field. Similarly, we maintain other parameters constant (Material A), except for the thermal expansion coefficient as $\alpha_1 = 3, 10, 20 \times 10^{-5\circ}\mathrm{C}^{-1}$. The critical speeds under the two deformation modes are shown in Figure 11.

A comparison between Figure 11(a) and (b) shows that the effects of the thermal expansion coefficient on the two deformation modes are quite different. For example, when α_1 increases, the symmetric solution increases correspondingly, while the anti-symmetric solution almost keeps constant.

To make a further investigation, we reproduce the results by using sufficiently small values of thermal expansion coefficient as follows $\alpha_1 = 3 \times 10^{-8\circ}\mathrm{C}^{-1}$ and $\alpha_1 = 3 \times 10^{-10\circ}\mathrm{C}^{-1}$, and the corresponding critical speeds are shown in Figure 12, in which the anti-symmetric solutions (solid lines) are lower throughout the entire range. Consequently, we can predict that the anti-symmetric mode is always dominant regardless of the coefficient of thermal expansion. In other words, the friction material thermal expansion coefficient has a negligible effect on the dominant deformation mode.

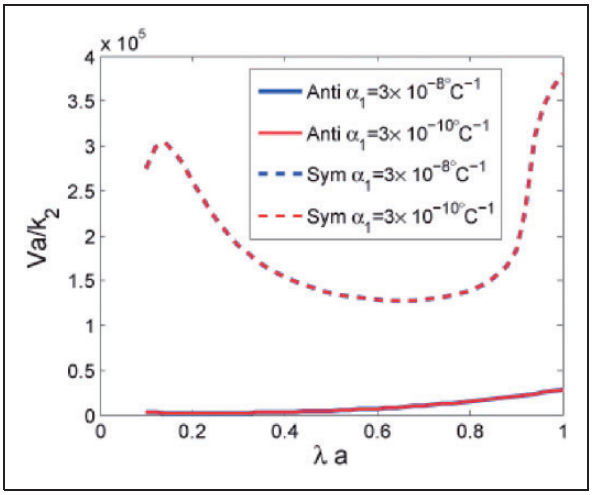

Figure 12. Critical speeds under two deformation modes with small friction material thermal expansion coefficient.

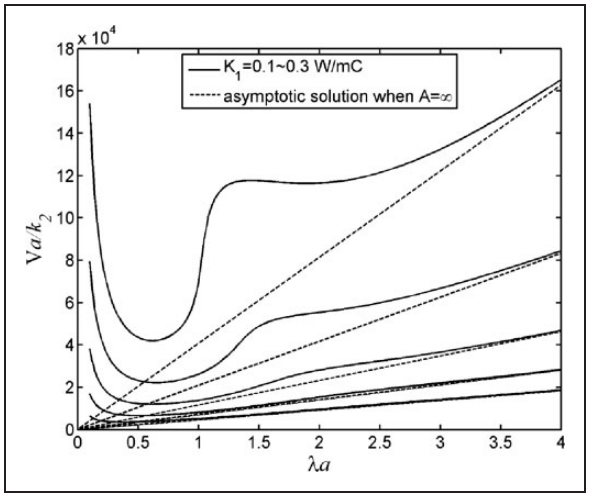

Figure 13. Asymptotic solution and Lee's symmetric solutions.

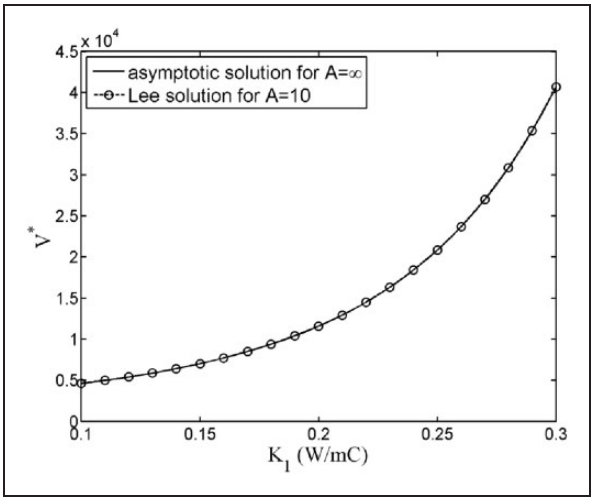

Figure 14. Comparison of Lee's solution at $A = 10$ with the asymptotic solution.

Asymptotic solution

Figure 13 is Lee's solution for K_1 varying between 0.1 and 0.3 W/m °C, along with the asymptotic solution for $A \to \infty$, which is determined from equation (20). To validate the asymptotic solution, Lee's solution of V^* at $A = 10$ is obtained as a function of K_1 and compared with equation (20), as shown in Figure 14. Again excellent agreements have been achieved. The result also indicates that the asymptotic solution is applicable for $A > 10$.

Conclusion

The effects of friction material properties on both the symmetric solution and the dominant deformation mode have been verified by the analytical and the FE approaches. The results show that the symmetric TE mode can become predominant in the condition when the friction material has either a large elastic modulus or a small thermal conductivity. Under these conditions, a transient state from the symmetric mode to the anti-symmetric mode can appear during frictional sliding. Moreover, the symmetric dominant region depends on the friction material properties. Meanwhile, the effect of the thermal expansion coefficient on the dominant TEI mode can be negligible.

Furthermore, the symmetric solution of the critical speed increases when the thermal conductivity or thermal expansion coefficient increases. By contrast, the symmetric solution decreases when the elastic modulus increases.

Acknowledgements

The authors would like to appreciate the helpful support given by Prof. JR Barber at the University of Michigan.

Conflict of interest

None declared.

Funding

This research received no specific grant from any funding agency in the public, commercial, or not-for-profit sectors.

References

1. Barber JR. Thermoelastic instabilities in the sliding of conforming solids. *Proc Roy Soc Lond Ser A* 1969; 312: 381–394.
2. Dow TA and Burton RA. Thermoelastic instability of sliding contract in the absence of wear. *Wear* 1972; 19: 315–328.
3. Lee SW and Jang YH. Effect of functionally graded material on frictionally excited thermoelastic instability. *Wear* 2009; 267: 1715–1722.
4. Afferrante L, Ciavarella M, Decuzzi G, et al. Thermoelastic instability in a thin layer sliding between two halfplanes: Transient behavior. *Tribol Int* 2003; 36: 205–212.
5. Zhao J, Ma B, Li H, et al. The effect of lubrication film thickness on thermoelastic instability under fluid lubricating condition. *Wear* 2013; 303: 146–153.
6. Anderson AE and Knapp RA. Hot spotting in automotive friction systems. In: *International conference on wear of materials*, vol. 2, 1989, pp.673–680.
7. Lee KJ and Barber JR. An experimental investigation of frictionally-excited thermoelastic instability in automotive disk brakes under a drag brake application. *ASME J Tribol* 1994; 116: 409–414.
8. Yeo T and Barber JR. Finite element analysis of thermoelastic contact stability. *J Appl Mech* 1994; 61: 919–922.
9. Du S, Zagrodzki P, Barber JR, et al. Finite element analysis of frictionally-excited thermoelastic instability. *J Therm Stress* 1997; 20: 185–201.
10. Yi YB, Barber JR and Zagrodzki P. Eigenvalue solution of thermoelastic instability problems using Fourier reduction. *Proc Roy Soc Lond Ser A* 2000; 456: 2799–2821.
11. Zagrodzki P and Truncone SA. Generation of hot spots in a wet multidisk clutch during short-term engagement. *Wear* 2003; 254: 474–491.
12. Lee H and Jang YH. Effect of the volume of a functionally graded material layer on frictionally excited thermoelastic instability. *Tribol Int* 2012; 49: 103–109.
13. Lee KJ and Barber JR. Frictionally-excited thermoelastic instability in automotive disk brakes. *ASME J Tribol* 1993; 115: 607–614.
14. Thoms E. Disc brakes for heavy vehicles. In: *International conference on disc brakes for commercial vehicles*, vol. C464, 1988, pp.133–137.
15. Decuzzi P, Ciavarella M and Monno G. Frictionally excited thermoelastic instability in multi-disk clutches and brakes. *ASME J Tribol* 2001; 123: 865–871.
16. Hartsock DL and Fash JW. Effect of pad/caliper stiffness, pad thickness, and pad length on thermoelastic instability in disk brakes. *ASME J Tribol* 2000; 122: 511–518.
17. Harding PRJ and Wintle BJ. Flexural effects in disc brake pads. *Proc Instn Mech Engrs* 1978; 192: 1–7.